FLEXOELECTRIC ROTATION OF POLARIZATION IN FERROELECTRIC THIN FILMS

G. Catalan[1,2*], A. Lubk[3], A.H.G. Vlooswijk[1], E. Snoeck[3, 5], C. Magen[5, 6], A. Janssens[4], G. Rispens[1], G. Rijnders[4], D.H.A. Blank[4] and B. Noheda[1†]

Institutions:

[1]Zernike Institute for Advanced Materials, University of Groningen, 9747 AG Groningen, The Netherlands.

[2]ICREA and CIN2, Campus Universitat Autonoma de Barcelona, Bellaterra 08193, Barcelona, Spain.

[3] CEMES-CNRS, 29, rue Jeanne-Marvig 31055 Toulouse, France

[4] MESA+ Institute for Nanotechnology, University of Twente, 7500 AE Enschede, The Netherlands.

[5] Transpyrenean Associated Laboratory for Electron Microscopy, CEMES – INA, CNRS – University of Zaragoza

[6] Instituto de Nanociencia de Aragón-ARAID and Departamento de Física de la Materia Condensada, Universidad de Zaragoza, 50018 Zaragoza, Spain.

Authors to whom correspondence should be addressed:

G. Catalan or B. Noheda

*E-mail address: gustau.catalan@cin2.es

†Email address: b.noheda@rug.nl

Abstract

Strain engineering allows modifying the properties of thin films using the stress from the substrates on which they are grown. Strain may be relaxed, however, and this can also modify the properties thanks to the coupling between strain gradient and polarization known as flexoelectricity. Here we have studied the strain distribution inside epitaxial films of the archetypal ferroelectric $PbTiO_3$, where the mismatch with the substrate is relaxed via the formation of domains (twins). Synchrotron X-ray diffraction and high-resolution transmission electron microscopy reveal an intricate strain distribution, with gradients both in the vertical and, unexpectedly, the horizontal direction. These gradients generate a horizontal flexoelectricity that forces the spontaneous polarization to rotate away from the normal. Polar rotations are a characteristic of compositionally engineered morphotropic phase boundary ferroelectrics with high piezoelectricity; flexoelectricity provides an alternative route for generating such rotations in standard ferroelectrics using purely physical means.

Introduction

In ferroelectric thin films, the coupling between strain and electrical polarization (piezoelectricity) is intrinsic and allows functional optimization by an adequate choice of substrate (strain engineering) [1-6]. It is only recently, however, that the important role of *strain gradients* has been highlighted [7-9]. Strain gradients couple to polarization in all dielectrics via *flexoelectricity* [10-20], which is large at the nanoscale because the size of the gradients is inversely proportional to the relaxation length –and hence to the sample size. Thus, in ferroelectric films and nanodevices, the local strain distribution is at least as important as the average strain value: it can modify the dielectric constant [7, 8] or cause imprint [20], it can be used to elicit piezoelectric-like responses in devices made out of non-piezoelectric materials [12, 13], and it can enhance the piezoelectric response of ferroelectric materials above their bulk value [15].

Present technologies enable the layer-by-layer growth of atomically flat ferroelectric films that are perfectly epitaxial and that, in the right conditions, may be largely free of dislocations [20]. Under these conditions, the available strain-relieving mechanisms are a change of symmetry [2, 22], the formation of ferroelastic domains [23], or both [24, 25]. In the absence of dislocations, and outside of the domain walls, one might expect the strain state of a film to be homogeneous.

However, the present work shows that large elastic strain gradients also occur in dislocation-free but ferroelastically twinned films. These strain gradients are intrinsic, as their origin is geometric, and long range (tens of nm). The gradient-induced polarization (flexoelectricity) is found to be large: several $\mu C/cm^2$, comparable to ferroelectricity. Moreover, the flexoelectricity is horizontal, and causes a rotation of the out-of-plane ferroelectricity in the c-domains. Gradient engineering through twinning thus provides an alternative route to the generation of ferroelectrics with rotated polarization, a feature thought to enhance piezoelectricity [26, 27, 28].

The samples studied here are thin films of $PbTiO_3$, with thickness of about 30 nm, grown on single crystal substrates of $DyScO_3$. $PbTiO_3$ is chosen as an aristotype of $Pb(Zr,Ti)O_3$, the most widely used material in piezoelectric transducers. Importantly, in its high temperature cubic phase, $PbTiO_3$ has an almost perfect lattice match with $DyScO_3$, enabling the growth of fully coherent films. As they cool down from the growth temperature, the films transform into the ferroelectric phase. In epitaxial $PbTiO_3$ grown on $DyScO_3$, different symmetries and domain structures may appear depending on the thickness. Ultra-thin films (5nm) display a periodic ferroelectric, non-ferroelastic, domain structure [22], while at larger thickness (>10nm), the misfit strain is relaxed by dividing the film into

tetragonal 90^{o} domains (a-c twins) that alternate in-plane and out-of-plane polarization [25, 30, 29, 31].

The ferroelectric domain structure of the films was characterized with piezo-response force microscopy. The phase contrast images (Figure 1) show the alternation of darker and brighter stripes, reflecting the vertical and horizontal polarization, respectively. The domain structures are therefore classic *a-c* twins, arranged in clusters or *bundles* [34].

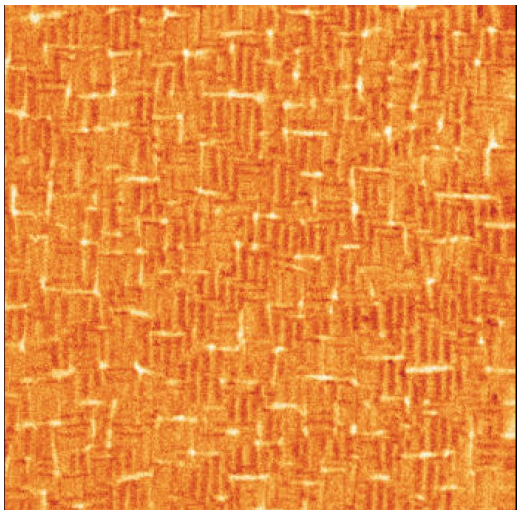

Figure 1. Piezo-response force microscopy image of a twinned ferroelectric film. The alternating dark and pale orange stripes correspond to narrow domains with polarization alternating between, respectively, the vertical and horizontal polarizations in a 30nm thick film of $PbTiO_3$ grown on a $SrRuO_3$-buffered $DyScO_3$. The image area is 2x2 microns.

In order to investigate the strain state, the lattice parameters of the film were mapped using synchrotron x-ray diffraction in grazing

incidence geometry. In this way, large diffracted intensities not limited by the finite thickness of the film can be collected, and the in-plane structure of the film can be characterized. In grazing incidence, the maximum intensity is obtained when the incident angle of the x-ray beam with the film surface, α_i, is close to the critical angle for total reflection[35], which is $\alpha_c \sim 0.29^o$ for for $PbTiO_3$ at the wavelength used (λ=1.265Å).

In figure 2a we observe that, when the incident angle is close to the nominal α_c, there is a diffraction maximum at about 37.5^o , corresponding to a lattice parameter that is very close to the substrate's. This broad maximum corresponds to the *c*-domains, which have polarization out of plane and thus a compressed in-plane lattice parameter. As α_i increases, a second peak appears at smaller angles (larger lattice parameters), corresponding to the *a*-domains, which have polarization in-plane and thus horizontal elongation. As the incident angle is further increased, the two diffraction maxima migrate away from each other, signalling a growing difference between the in-plane *a* and *c* lattice parameters.

This evolution with incidence angle reflects a distribution of crystallographic inclination angles within the domains [36]. In bulk tetragonal twinning, the Bragg planes of adjacent a and c domains form an angle (figure 2b) that is given by:

$$\gamma = 2\arctan(c/a) - 90^{o} \quad \textbf{(1)}$$

This relative angle should be 3.6 degrees for a fully relaxed $PbTiO_3$, but in the films the tetragonality c/a is inhomogeneous (as indicated by the X-rays), resulting in a distribution of Bragg plane inclinations. The regions with different local inclinations meet the Bragg condition at different incidence angles (α), and thus the diffraction data reveal the correlated distribution of tetragonality and twinning angle, in agreement with equation 1. This can also be observed in the out-of-plane diffraction maps around the 00L reflections (figure 2c).

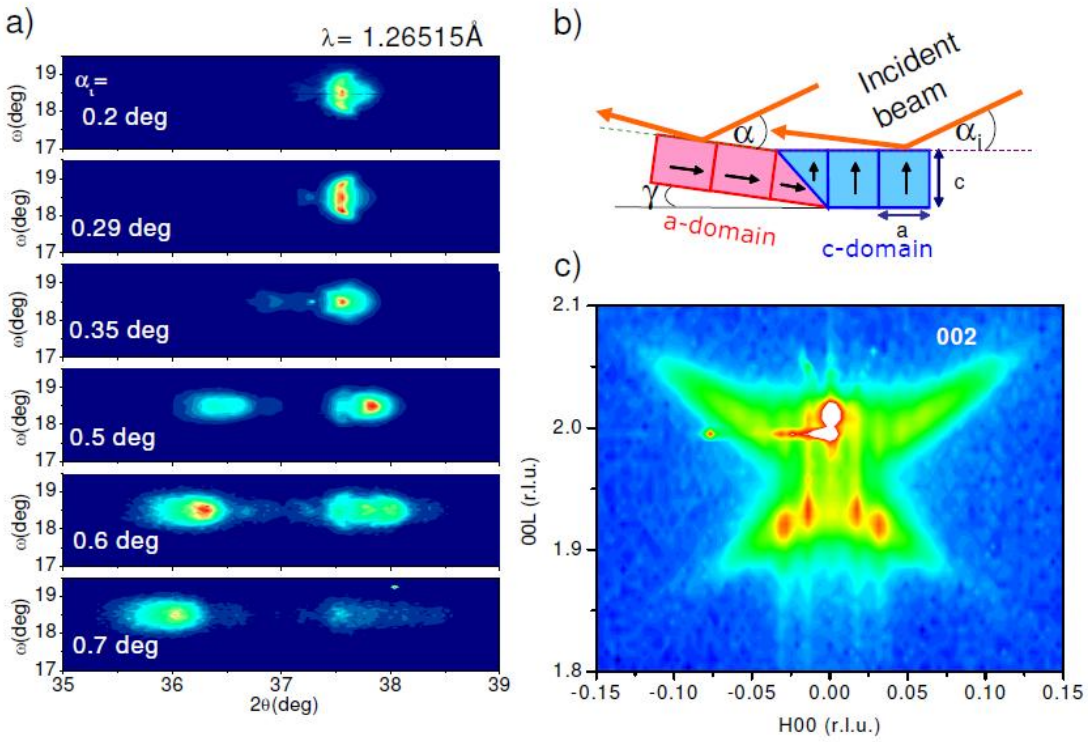

Figure 2. X-ray diffraction data revealing a correlated distribution of tetragonality and twin angles: (a) Reciprocal space maps as a function of grazing incidence angle, and (b) schematic representation of fully relaxed tetragonal domains, showing the relative Bragg plane

inclination. Notice that the real incidence angle for the a-domains, α, is different from the nominal one (α_i) due to the tetragonal inclination angle, γ: i.e., $\alpha = \alpha_i - \gamma$, with γ being biggest in the very thin *a*-domains (c) Reciprocal space map around the (002) reflection, where the intensity outside the 00L vertical is due to the distribution of crystallographic inclination within the a-domains (L>2) as well as the c- domains (L<1.95) with respect to the substrate planes (L≡2).

Further insight can be gained by probe-corrected High-Angle Annular Dark Field Scanning TEM (HAADF-STEM) imaging [40, 41], shown in Figure 3. Quantitative analysis of the HRSTEM images using the Geometric Phase Analysis (GPA) [38, 39] and using the $DyScO_3$ substrate as reference shows that the there is a vertical gradient of inclinations between the flatter bottom interface and the more rumpled free surface, reflecting the growing distance to the interface, which is the source of stress. More unexpectedly, however, the films also show *horizontal* strain gradients. The c-domains, for example, reveal an increased out-of-plane elongation in the acute interfacial corners, and a reduced tetragonality in the obtuse ones.

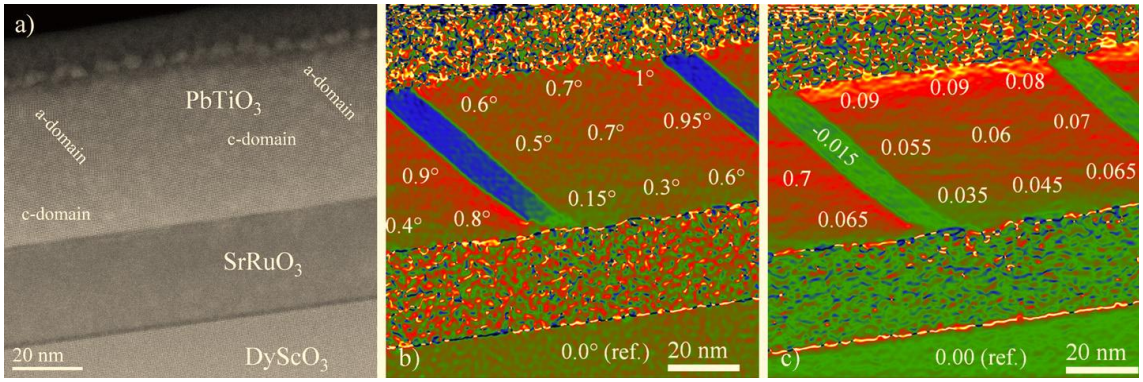

Figure 3: **Direct imaging of strain gradients by HRTEM** High resolution scanning TEM and geometric phase analysis (GPA) of the $PbTiO_3$ thin film grown on a $SrRuO_3$ buffer layer deposited on $DyScO_3$ substrate and studied in cross-section. (a) HRTEM image, showing the structure. (b) The map of lattice rotations shows that the upper layers are more relaxed, and therefore more inclined, than those close to the interface. (c) The out-of-plane strain ε_{zz} (relative to the $DyScO_3$ substrate, c= 3.95Å) shows a higher tetragonality in the right of the c-domain than in the left (obtuse). The difference arises from the the local stress concentrations required in order to "flatten" the interface of the ferroelastic film onto the substrate, as shown in figure 5.

This distinctive pattern can be understood by consideration of the deformations that are required in order to attach a film with ferroelastic domains onto the flat surface of the substrate, as depicted in **figure 4-a**. A useful analogy is to imagine the forces needed to flatten an open book onto a photocopier. The concentration of stress at the corners of the domains leads to locally enhanced deformations, including bending of the domain walls in order to preserve coherence, as observed. Yet another way to understand the strain difference is to consider that, while the bottom interface must

be flat, the top interface is freer to relax towards its natural "rumpled" state with inclined planes: the net result is that, for each domain, one side is thicker than the other (see **figure 4-b**), and thus there is a horizontal gradient of vertical expansion. This transverse gradient will generate a horizontal flexoelectricity, causing the vertical polarization to rotate towards the thicker side (**figure 4-b**.)

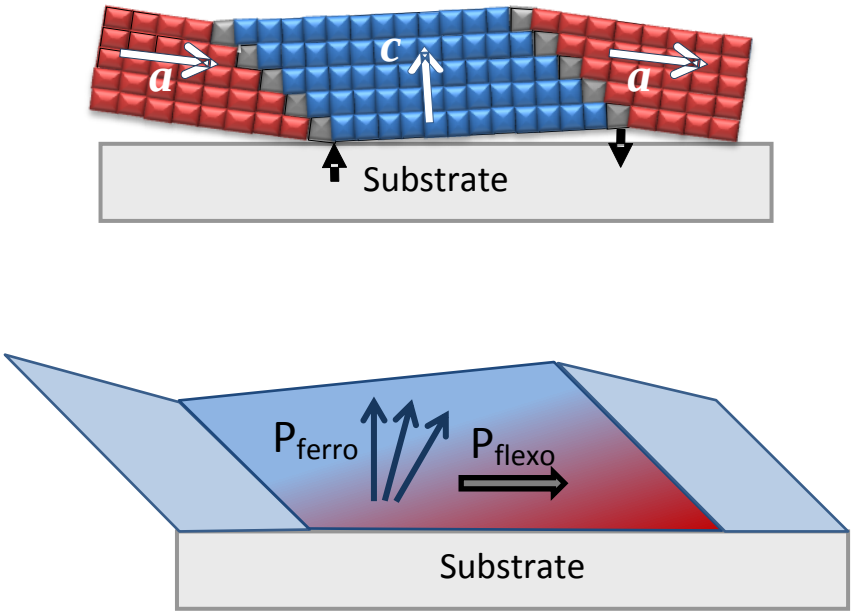

Figure 4. Sketch of stresses, strain gradients and polar vectors in the twinned film: (a) Schematic representation of the domain structure in a film with a-c domains. The black arrows represent the stresses that must be applied to the twinned film in order to flatten it onto the substrate. (b) the flexoelectric polarization (grey) induces a rotation of the ferroelectric polarization of the c-domain (blue).

We can estimate the horizontal flexoelectricity and its effect on the spontaneous polarization. The transverse flexoelectric coefficient of

lead zirconate-titanate is $f_{13} \sim 1$ μC/m [44]. Flexoelectricity is proportional to permittivity [7,10,12,17], which is ~5 times smaller for pure lead titanate than for lead zirconate-titanate [45], so the transverse flexoelectric coefficient of $PbTiO_3$ should be less than $f_{13} \approx$ 200nC/m. The out-of-plane strain difference between the acute and obtuse corners of the c-domains is $\Delta\varepsilon_3 \approx 0.03$ (figure 3-c), and the relaxation length is approximately the *c*-domain width ($w \approx$ 40nm). Therefore, the average horizontal flexoelectricity across the domain should be around $\boldsymbol{P}_{\mathbf{x(\underline{flexo})}} \cong f_{13}\frac{\Delta\varepsilon_3}{w} \approx 15\mu C/cm^2$.

This flexoelectric polarization is very large; it is in fact comparable to the spontaneous polarization of archetypal ferroelectrics, and will therefore have a strong effect on them. In particular, the addition of the horizontal flexoelectricity to the vertical ferroelectricity of the c-domains will result in a rotated polarization (see **figure 4-b**), with an angle, β, given by: $\tan\beta = P_{flexo}/P_{ferro}$. Using $P_{flexo} \sim 15\mu C/cm^2$ and P_{ferro}=40-60μC/cm^2, an average polar rotation of $\beta \sim 10\text{-}15^o$ expected with respect to the normal direction.

In order to test this prediction, accurate measurements of lattice distortions were performed by increasing the STEM resolution and performing dedicated model-based peak finding in order to determine atomic column positions. Based on the Z-dependent contrast, Pb and

TiO columns can be easily distinguished, while weakly scattering O columns are not visible (see **figure 5a**). Based on the determined Pb and TiO column positions, both the strain tensor and the Pb-TiO distance vector (proportional to the electric polarization via the Born effective charge tensor[42]) are mapped unit-cell-wise (see **figure 5b**). Polarization mapping can also be done by other high resolution TEM techniques [43], although HAADF has the advantage that the samples need not be so thin and the less aggressive sample preparation helps preserve the native domain structure [41].

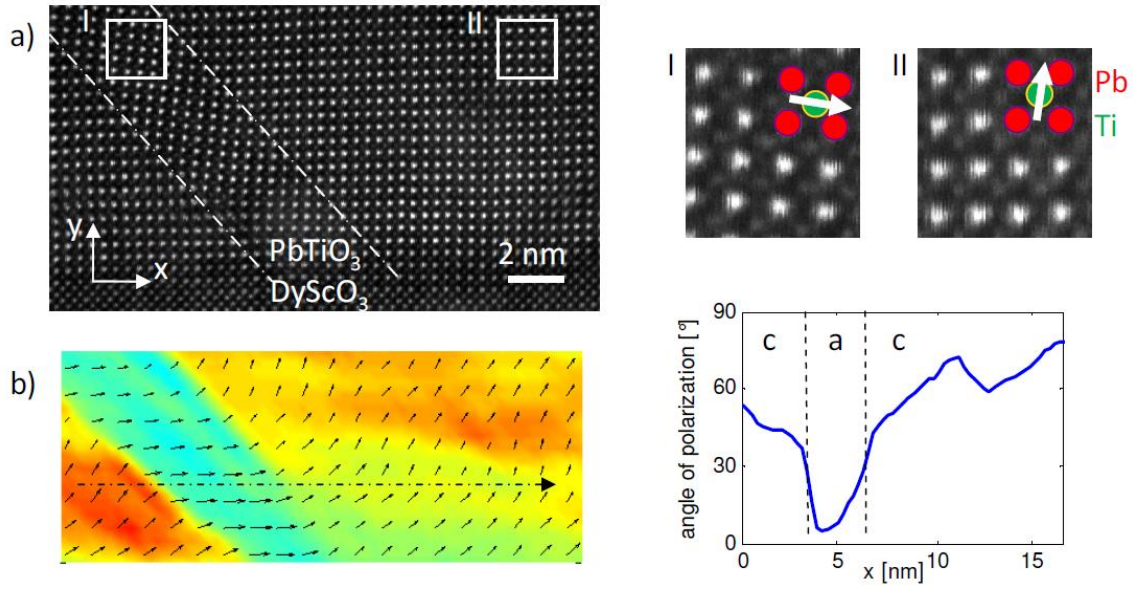

Figure 5. Direct observation of polarization rotations: a) HAADF STEM image with zoom-ins showing the a-domain (I) and c-domain (I) atomic column arrangement with the TiO column shifted off-center along the direction of polarization. b) Out-of-plane strain (color map) and electric polarization (vector map). The map confirms the strain difference between acute and obtuse corners and reveals the existence of polar rotations in the c-domains, which are quantified

in the line scan; the rotation angle away from the normal is bigger than 10 degrees throughout the entire domain, in good agreement with the calculations.

In agreement with the HRSTEM GPA, one observes a large difference in out-of-plane strain, tensile in the acute corners and compressive in the obtuse ones, leading to a horizontal gradient. Additionally, a strong rotation of the electric polarization (much bigger than the Bragg plane inclination) is observed in the c-domain (see vectorial map and linescan in Fig 5-b). Inspection of figure 5b confirms a polar rotation of the order of 10° in the middle of the c-domain, in agreement with our model. The rotation is even bigger near its corners, where the gradient is strongest, and also near the interface, where the vertical polarization is reduced [43]. We notice also that there is no significant polar rotation in the a-domains, also in agreement with our model: in the a-domains the polarization is already horizontal, so the addition of horizontal flexoelectricity can change its magnitude but not its angle.

The observed rotation of the polarization vector implies that the internal symmetry of the unit cells is lower than tetragonal, even though the X-rays do not evidence any monoclinic distortion of the unit cell. This may be due to the small coherence length of the domains, or else it might indicate that the unit cells remainin "metrically tetragonal" in spite of their lower internal symmetry.

Decoupling between tetragonality and polarization is a known feature of epitaxial thin films, which remain tetragonal even when the polarization is suppressed [43, 46].

Symmetry lowering via polar rotation is thought to be a cause for the giant piezoelectricity of PZT and other ferroelectrics compositionally engineered to be near a morphotropic phase boundary [26, 27, 28]. Nanodomain formation is in fact intrinsic near such boundaries [47], so it is quite possible that controversies regarding their symmetry [47-49] be related to the existence internal flexoelectricity, seen also in relaxors[50]. Transverse permittivity is bigger than longitudinal one in $PbTiO_3$ [45], so the net rotation away from the vertical direction should result in an enhancement of out-of-plane permittivity and piezoelectricity. Though the enhancement will be hindered by clamping, focussed ion beam patterning of individual clusters of domains can reveal it [51].

Flexoelectricity thus offers a way to induce polar rotations in non-morphotropic ferroelectrics using purely physical means. The size of the gradients is inversely proportional to the domain size, which can be tuned by changing the film thickness or the film/substrate combination (29, 30). Moreover, flexoelectric coefficients are thought to be larger for lead-free ferroelectrics than for lead-containing ones

[12], which has positive implications in the quest for large lead free piezoelectricity.

METHODS

The thin films have been deposited by pulsed laser deposition (PLD), using a Lambda Physik COMPex Pro 205 KrF (λ=248 nm) excimer UV laser and a TSST-RHEED vacuum system. The background pressure was 10^{-8} mbar. The $PbTiO_3$ targets were 2-8% Pb-enriched sintered ceramics. The target-substrate distance was 48mm. The growth took place at a substrate temperature of 570 °C, with a laser energy density of 2 J/cm^2, a laser repetition rate of 1 Hz and under an oxygen pressure of 0.13 mbar. The laser spot size on the target was 0.76 mm^2. The substrates were pre-deposition treated in order to ensure a single substrate termination [52], and a $SrRuO_3$ layer was added as a buffer to aid growth and as an electrode to facilitate functional measurements with piezoresponse force microscopy. The $SrRuO_3$ layers had thicknesses ranging from 5 to 15nm and were in-plane coherent with the substrate. The films have been characterized using atomic force microscopy, (AFM), piezoresponse-AFM, grazing incidence X-ray diffraction (GIXRD) and high resolution (scanning) transmission electron microscopy (HRTEM). The AFM measurements have been performed on Agilent 5100 and 5500 AFM systems. For our XRD measurements we have used both the facilities of the HASYLAB W1 beamline (DESY, Hamburg) and a Panalytical X'Pert MRD Cradle (four axes) lab diffractometer. Our lab diffractometer is equipped with a copper X-ray generator tube, supplying X-rays with λ=1.5406Å (Cu Kα). The photon energy used at the W1 beamline is 9800eV, corresponding to a wavelength of λ=1.2651Å.

The samples for the STEM experiments were prepared in cross section following the standard method: they were first manual tripod-polished down to ~20 microns then

finally thinned down to the electron transparency using a Gatan PIPS© ion milling system. STEM HAADF studies were carried out on a Titan 60-300 kV microscope (FEI) fitted with a high brightness field emission gun (X-FEG) and a probe Cs corrector from CEOS. The convergence angle of 25 mrad yields a probe size of less than 0.10 nm. The scanning distortion was minimized by acquiring and superimposing two perpendicularly scanned images. Displacement and strain fields were deduced for the HRSTEM micrographs using the Geometrical Phase Method (GPA) [38, 39].

Model-based structure analysis was performed by maximum likelihood fitting of a bivariate Gaussian plus background to each atomic column contrast. Cross-talk between atomic columns was approximately taken into account by starting the procedure at the strongest column contrast and subsequently fitting the weaker ones by taking into account the tails of the previously determined Gaussians. The colour map in Figure 5-c was smoothed using an averaging window of 1.6nm.

Acknowledgement

Wolfgang Caliebe is gratefully acknowledged for his help at the W1 beamline. This work is part of the research programme 04PR2359 of the Foundation for Fundamental Research on Matter (FOM), which is part of the Netherlands Organisation for Scientific Research (NWO). G.C., A.H.G.V. and B.N. also acknowledge financial support from the NWO-Vidi grant 700.54.426, and from the Explora grant MAT2010-10067-E (G.C.). A.L. and E.S. acknowledge financial support from the European Union under the Framework 6 program under a

contract for an Integrated Infrastructure Initiative. Reference 026019 ESTEEM.

Author contributions:

G.C. and B.N. have devised, designed and organized the work; A.H.G.V and A. J. have grown the films under the supervision of G.R. and D.H.A.B.; A.H.G.V, G.C., G.R. and B.N. have performed the x-ray experiments and analysed the x-ray data; A. L., E.S., and C. M. have designed, performed and organized the electron microscopy experiments and analysed the data. All the authors have contributed to the discussions.

REFERENCES

1. G. A. Rossetti, L. E. Cross, and K. Kushida, Stress induced shift of the Curie point in epitaxial $PbTiO_3$ thin films, *Appl. Phys. Lett.* 59, 2524 (1991).
2. N.A. Pertsev, A.G. Zembilgotov and A.K. Tagantsev, Effect of Mechanical Boundary Conditions on Phase Diagrams of Epitaxial Ferroelectric Thin Films, *Phys. Rev. Lett.* 80, 1988-1991 (1998).
3. C.L. Canedy, Hao Li, S. P. Alpay, L. Salamanca-Riba, A. L. Roytburd, and R. Ramesh, Dielectric properties in heteroepitaxial $Ba_{0.6}Sr_{0.4}TiO_3$ thin films: Effect of internal stresses and dislocation-type defects, *Appl. Phys. Lett.* 77, 1695-1697 (2000).

4. L.J. Sinnamon, R.M. Bowman and J.M. Gregg, Thickness-induced stabilization of ferroelectricity in SrRuO3/Ba0.5Sr0.5TiO3/Au thin film capacitors, *Appl. Phys. Lett.* 81(5), 889-891 (2002).
5. K.J. Choi, M. Biegalski, Y. L. Li, A. Sharan, J. Schubert, R. Uecker, P. Reiche, Y. B. Chen, X. Q. Pan, V. Gopalan, L.-Q. Chen, D. G. Schlom, and C. B. Eom, Enhancement of Ferroelectricity in Strained $BaTiO_3$ Thin Films, *Science* 306, 1005 (2004).
6. J.H. Haeni, P. Irvin, W. Chang, R. Uecker, P. Reiche, Y. L. Li, S. Choudhury, W. Tian, M. E. Hawley, B. Craigo, A. K. Tagantsev, X. Q. Pan, S. K. Streiffer, L. Q. Chen, S. W. Kirchoefer, J. Levy, and D. G. Schlom, Room-temperature ferroelectricity in strained $SrTiO_3$, *Nature* 430, 758 (2004).
7. G. Catalan, L.J. Sinnamon and J.M. Gregg, The effect of flexoelectricity on the dielectric properties of inhomogeneously strained ferroelectric thin films, *J. Phys.: Cond. Mat.* 16, 2253-2264 (2004).
8. G. Catalan, B. Noheda, J. McAneney, L. J. Sinnamon, and J. M. Gregg, Strain Gradients in Epitaxial Ferroelectrics, *Phys. Rev. B* 72, 020102 (2005).
9. M.S. Majdoub, R. Maranganti and P. Sharma, Understanding the origins of the intrinsic dead layer effect in nanocapacitors, *Phys. Rev. B* 79, 115412 (2009).
10. V.D. Kogan, Piezoelectric effect during inhomogeneous deformation and acoustic scattering of carriers in crystals, *Sov. Phys. Solid. State* 5, 2069 (1964).

11. E. V. Bursian, O. I. Zaikovskii, Changes in the curvature of a ferroelectric film due to polarization, *Sov. Phys. Sol. State* 10, 1121 (1968).
12. L.E. Cross, Flexoelectric effects: Charge separation in insulating solids subjected to elastic strain gradients, *J. Mat. Sci.* 41, 53-63 (2006).
13. W. Zhu, J. Y. Fu, N. Li, and L. Cross, "Piezoelectric composite based on the enhanced flexoelectric effects", Appl. Phys. Lett. **89**, 192904 (2006).
14. W. Ma, A study of flexoelectric coupling associated internal electric field and stress in thin film ferroelectrics, *Phys. Stat. Sol*. (b) 245, No. 4, 761–768 (2008).
15. M. S. Majdoub, P. Sharma, and T. Çağin, Dramatic enhancement in energy harvesting for a narrow range of dimensions in piezoelectric nanostructures, Phys. Rev. B 78, 121407 (2008).
16. A. K. Tagantsev, V. Meunier, P. Sharma, Novel Electromechanical Phenomena at the Nanoscale: Phenomenological Theory and Atomistic Modeling, *MRS Bullettin* 34, 643 (2009).
17. P. Zubko G. Catalan, P. R. L. Welche, A. Buckley, and J. F. Scott, Strain-Gradient-Induced Polarization in $SrTiO_3$ Single Crystals, *Phys. Rev. Lett.* 99, 167601 (2007); ibid, *Phys. Rev. Lett.* 100 199906 (2008).
18. R. Maranganti and P. Sharma, Atomistic determination of flexoelectric properties of crystalline dielectrics, *Phys. Rev. B* 80, 054109 (2009).
19. J. Hong, G. Catalan, J. F. Scott and E. Artacho, The flexoelectricity of barium and strontium titanates from first principles, *Journal of Physics: Condensed Matter* 22, 112201 (2010).

20. A. Gruverman, B.J. Rodriguez, R.J. Nemanich, A.I. Kingon, A. Tagantsev, J.S. Cross and M. Tsukada "Mechanical Stress Effect on Imprint Behavior of Integrated Ferroelectric Capacitors", Appl. Phys. Lett. 83, 728-730 (2003); A. K. Tagantsev, L. E. Cross and J. Fousek, Domains in Ferroelectric Crystals and Thin Films, Springer, New York, 2010, p.637.; D. Lee, A. Yoon, S. Y. Jang, J.-G. Yoon, J.-S. Chung, M. Kim, J. F. Scott, and T. W. Noh, Phys. Rev. Lett. 107, 057602 (2011).
21. I. Vrejoiu, G. Le Rhun, L. Pintilie, D. Hesse, M. Alexe, U. Gösele, Intrinsic ferroelectric properties of strained tetragonal $PbZr_{0.2}Ti_{0.8}O_3$ obtained on layer-by-layer grown, defect-free single-crystalline films, *Adv. Mat.* 18, 1657 (2006).
22. G. Catalan, A. Janssens, G. Rispens, S. Csiszar, O. Seeck, G. Rijnders, D. H. A. Blank, and B. Noheda, Polar Domains in Lead Titanate Films under Tensile Strain, *Phys. Rev. Lett.* 96, 127602 (2006).
23. W. Pompe, X. Gong, Z. Suo, and J. S. Speck, Elastic energy release due to domain formation in the strained epitaxy of ferroelectric and ferroelastic films, *J. Appl. Phys.* 74, 6012-6019 (1993).
24. R. J. Zeches, M. D. Rossell, J. X. Zhang, A. J. Hatt, Q. He, C.-H. Yang, A. Kumar, C. H. Wang, A. Melville, C. Adamo, G. Sheng, Y.-H. Chu, J. F. Ihlefeld, R. Erni, C. Ederer, V. Gopalan, L. Q. Chen, D. G. Schlom, N. A. Spaldin, L. W. Martin, R. Ramesh, A Strain-Driven Morphotropic Phase Boundary in $BiFeO_3$, *Science* 326, 977 – 980 (2009).
25. Q.Y. Qiu, V. Nagarajan, S.P. Alpay, Film thickness versus misfit strain phase diagrams for epitaxial $PbTiO_3$ ultrathin ferroelectric films, *Phys. Rev. B* 78, 064117 (2008).

26. L. Bellaiche, A. Garcia and D. Vanderbilt, Finite-temperature properties of Pb(Zr1-xTix)O-3 alloys from first principles, Phys. Rev. Lett. 84, 5427 (2000).
27. H. Fu and R.E. Cohen, Polarization rotation mechanism for ultrahigh electromechanical response in single-crystal piezoelectrics, Nature 403, 281 (2000).
28. R. Guo, L. E. Cross, S. E. Park, B. Noheda, D.E. Cox and G. Shirane, Origin of the high piezoelectric response in $PbZr_{1-x}Ti_xO_3$, Phys. Rev. Lett. 84, 5423-5426 (2000).
29. J. S. Speck and W. Pompe, Domain configurations due to multiple misfit relaxation mechanisms in epitaxial ferroelectric thin films. I. Theory. *J. Appl. Phys.* 76, 466-476 (1994).
30. N.A. Pertsev and A.G. Zembilgotov, Energetics and geometry of 90° domain structures in epitaxial ferroelectric and ferroelastic films, *J. Appl. Phys.* 78(10), 6170-6180 (1995).
31. A. H. G. Vlooswijk, B. Noheda, G. Catalan, A. Janssens, B. Barcones, G. Rijnders, D. H. A. Blank, S. Venkatesan, B. Kooi, and J. T. M. de Hosson, Smallest 90° domains in epitaxial ferroelectric films, *Appl. Phys. Lett*. 91(11), 112901 (2007).
32. B. S. Kwak, A. Erbil, B. J. Wilkens, J. D. Budai, M. F. Chisholm, and L. A. Boatner, Strain relaxation by domain formation in epitaxial ferroelectric thin films, Phys. Rev. Lett. 68, 3733–3736 (1992);
33. B. S. Kwak, A. Erbil, J. D. Budai, M. F. Chisholm, L. A. Boatner, and B. J. Wilkens, Domain formation and strain relaxation in epitaxial ferroelectric heterostructures, Phys. Rev. B 49, 14865-14879 (1994).

34. Y. Ivry, D.P. Chu, C. Durkan, Bundles of polytwins as meta-elastic domains in the thin polycrystalline simple multi-ferroic system PZT, *Nanotechnology* 21, 065702 (2010).
35. U. Pietsch, V. Holy, T. Baumbach, "High-Resolution X-Ray Scattering: from thin films to lateral nanostructures", Springer-Verlag (New York, 2004).
36. Given that increasing the incidence angle increases the penetration depth of the X-rays [35], it is tempting to assign the increased tetragonality to lattice planes that are deeper [37]. However, it makes little physical sense that the least cubic parts of the film should be those closest to the substrate. Moreover, all the change in our films happens at angles above the critical incidence one, for which the X-ray penetration depth is already larger than the entire thickness of the film (as confirmed by the observation of the substrate peak).
37. D. Walker, P.A. Thomas, S.R. Collins, A comprehensive investigation of the structural properties of ferroelectric $PbZr_{0.2}Ti_{0.8}O_3$ thin films grown by PLD, *Phys. Stat. Solidi A* 206, 1799-1803 (2009).
38. M.J. Hytch, E. Snoeck and R. Kilaas, Quantitative measurement of displacement and strain fields from HREM micrographs, *Ultramicroscopy*, 74, pp. 131-146, (1998)
39. GPA Phase plug-in for DigitalMicrograph (Gatan) available from HREM Research Inc.: http://www.hremresearch.com.

40. P.D. Nellist, M.F. Chisholm, N. Dellby, O.L. Krivanek, M.F. Murfitt, Z.S. Szilagyi, A.R. Lupini, A. Borisevich, W.H. Sides Jr., S. J Pennycook, Science 305, 1741 (2004).
41. C. T. Nelson, B. Winchester, Yi Zhang, S.-J. Kim, A. Melville, C. Adamo, C. M. Folkman, S.-H. Baek, C.-B. Eom, D. G. Schlom, L.-Q. Chen, and X. Pan, "Spontaneous Vortex Nanodomain Arrays at Ferroelectric Heterointerfaces", Nano Letters 11, 828–834 (2011).
42. R. E. Cohen, Origin of ferroelectricity in perovskite oxides, Nature **358**, 136-138.
43. C.-L. Jia, V. Nagarajan, J.-Q. He, L. Houben, T. Zhao, R. Ramesh, K. Urban & R. Waser, "Unit-cell scalemapping of ferroelectricity and tetragonality in epitaxial ultrathin ferroelectric films" Nature Materials 6, 64 (2007).
44. W. Ma, L.E. Cross, Strain-gradient-induced electric polarization in lead zirconate titanate ceramics, *Appl. Phys. Lett.* 82, 3293 (2003).
45. K.-H. Hellwege, A. M. Hellwege, Eds., Landolt-Bornstein: Numerical Data and Functional Relationships in Science and Technology (Springer, Berlin, 1981), New Series–Group III, vol. 16a.
46. P Muralt, The emancipation of ferroelectricity, Nature Materials 6, 8 (2007).
47. G. A. Rossetti, Jr., Wei Zhang, and A. G. Khachaturyan, Phase coexistence near the morphotropic phase boundary in lead zirconate titanate ($PbZrO_3$-$PbTiO_3$) solid solutions, Appl. Phys. Lett. 88, 072912 (2006).
48. B Noheda, DE Cox, "Bridging phases at the morphotropic boundaries of lead oxide solid solutions" Phase Transitions 79, 5 (2006).

49. M. Davis, "Picturing the elephant: Giant piezoelectric activity and the monoclinic phases of relaxor-ferroelectric single crystals" J. Electroceramics 19, 23 (2007).
50. S. J. Ahn, J-J Kim, J-H Kim, and W-K Choo, "Origin of polar domains in ferroelectric relaxors", J. Kor. Phys. Soc. 42, S1009-S1011 (2003).
51. V. Nagarajan, A. Roytburd, A. Stanishevsky, S. Prasertchoung, T. Zhao, L. Chen, J. Melngailis, O. Auciello & R. Ramesh, "Dynamics of ferroelastic domains in ferroelectric thin films", Nature Materials 2, 43 - 47 (2003).
52. G. Koster, B. L. Kropman, G. J. H. M. Rijnders, D. H. A. Blank, and H. Rogalla, Quasi-ideal strontium titanate crystal surfaces through formation of strontium hydroxide, Appl. Phys. Lett. 73(20), 2920 (1998).